Pergamon

Cement and Concrete Research 30 (2000) 1915–1927

CEMENT AND CONCRETE RESEARCH

# Spalling and pore pressure in HPC at high temperatures

Pierre Kalifa*, François-Dominique Menneteau, Daniel Quenard

*Centre Scientifique et Technique du Bâtiment, 24 rue J. Fourier, 38400 St. Martin d'Hères, France*

Received 12 October 1999; accepted 1 August 2000

**Abstract**

High-performance concrete (HPC) are subject to spalling under certain thermal and mechanical conditions. Spalling results mainly from two processes: a "thermo-mechanical" process in which the stress originates in the gradients of thermal deformation within the material, and a thermo-hydral process where spalling is due to the build-up of gas pressure fields in the porous network. This paper deals with the thermo-hydral process. An original device was designed in order to make simultaneous measurements of pressure and temperature at various positions in a concrete specimen ($30 \times 30 \times 12$ cm$^3$) heated on one face up to 800°C. The specimen was also continuously weighed during the tests, thus, the mass loss, resulting mainly from water transport and loss, was recorded. This campaign was carried out on an ordinary concrete (OC) and a HPC (90 MPa). As expected, the pressure peaks were much higher than in HPC (40 bars) than in OC (20 bars). In HPC, these pressures exceeded the saturated vapor pressure. It is demonstrated that the thermal expansion of liquid water and the transport of water towards the inner part of the specimen play a significant role on the build-up of gas pressure. The experimental correlation between the pressure peaks and the plateau in the temperature curves confirmed the hypothesis that the drying front is preceded by a quasi-saturated layer that acts as a moisture clog. 

*Keywords:* Spalling; Pore pressure; High-performance concrete; Fire behavior; Mass loss

## 1. Introduction

During the last 20 years, concrete have evolved to provide better performances and also to a greater specialization in their field of application. The changes made in the composition of the mixes (reduction of water content, use of superplasticizers, optimization of grain size distribution, use of particles with pozzolanic activity, addition of fibers, etc.) lead to striking improvements in many properties such as strength, early strength increase, rheology of fresh concrete, ductility and compactness. The latter yields in most cases a better durability, but it may also lead to a brittle behavior of high-performance concrete (HPC) in fire conditions [1–7]: Under certain thermal and mechanical stresses, HPC may spall. Small scales fall out from the surface of the structure, and the process is repeated as long as conditions are met (progressive spalling); the concrete element may also suddenly fail with a very large release of energy (explosive spalling) [1,8]. In both cases, the integrity and load-bearing capacity of the structure may be jeopardized, reinforcing bars directly exposed to fire or complete failure of the element. Recent fires like under the Channel tunnel showed that the damage could be very serious. The high compactness of HPC is the main parameter responsible for spalling at high temperature. However, as we shall see later, many other parameters are involved.

Therefore, the designer has at his disposal a large variety of concretes for specific applications (workability, strength, permeability, etc.), but he has to take into account a possible brittle behavior of the structure at high temperature. Since the safety of people (inhabitants, firemen) is involved, the question has to be addressed very seriously. However, the brittle behavior of HPC as a material should not lead to the conclusion that HPC cannot be used in constructions. Several technological solutions should be considered:

- Restrict the use of HPC to zones where the risk of fire exposure is very low (e.g. foundations), or where the safety impact is low.

* Corresponding author. Tel.: +33-4-76-76-25-55; fax: +33-4-76-76-25-60.

*E-mail address*: kalifa@cstb.fr (P. Kalifa).

0008-8846/00/$ – see front matter 
PII: S0008-8846(00)00384-7

- Modify the microstructure of the material. The only solution currently used, besides mixture proportioning, is adding organic fibers (mainly polypropylene). It was implemented in several constructions such as the Japan Center in Frankfurt (Germany) [9].
- Improve the design of the structural element: dimensions, type of reinforcement, external protection, etc.
- Modify the design of the construction itself, so that the thermal stress on the HPC elements is lower.

In other words, with these new materials, both more effective and more specialized, a new and global approach of building design is required. Addressing the question of fire behavior should consider the development of technological solutions at all four levels mentioned above.

This global approach has to be supported by a good understanding and simulation of the processes involved in the material at high temperature. This modeling is considered as a basis tool for predicting and preventing the fire behavior of structures.

In the first part of this paper, after a short description of the processes leading to spalling, a state of the art will describe the methodologies currently used to model, characterize and predict the behavior of concrete elements and structures under thermal and mechanical solicitations. The second part deals with the measurement of pore pressure and temperature fields, as well as mass loss in concrete specimens subjected to a quasi-unidirectional heat solicitation. As we shall see in the following, the build-up of high pore pressures is one of the major factors responsible for spalling. The original set-up developed therefore provides very worthwhile information to understand the spalling phenomenon.

## 2. Background: simulation and characterization of spalling

### 2.1. The physical processes relevant to spalling

Spalling results from two main concomitant processes: the first one is related to the thermal dilation gradients taking place in the structure element (thermo-mechanical process); the second one (the thermo-hydral process) is associated with the transfer of mass in the porous network (air, vapor, liquid water), which results in the build-up of high pore pressures and pore pressure gradients. Whether one or the other is dominant depends notably on the thermal solicitation. Spalling therefore results from a thermo-hydro-mechanical coupled process.

The thermo-mechanical process is directly associated with the temperature field in the concrete element [10]. The temperature gradients induce gradients of thermal dilation, which in turn generate tensile stresses perpendicular to the heated face. Local strain incompatibilities between the cement paste and the aggregates also exist: While the aggregates dilate with increasing temperature until they are chemically degraded [11], the cement paste shrinks as soon as it looses water (by drying and dehydration) [3,12,13]. The chemical degradation of the paste mainly starts from 180°C [12,14]. This differential thermal behavior is an important source of matrix degradation, as observed in SEM images [14].

The thermo-hydral process is associated with the transfer of mass (water in liquid and vapor phases and air), as illustrated in Fig. 1 [15,16]. As temperature increases, water is partly evaporated. This evaporation generates a pressure in the porous network. The pressure gradient is

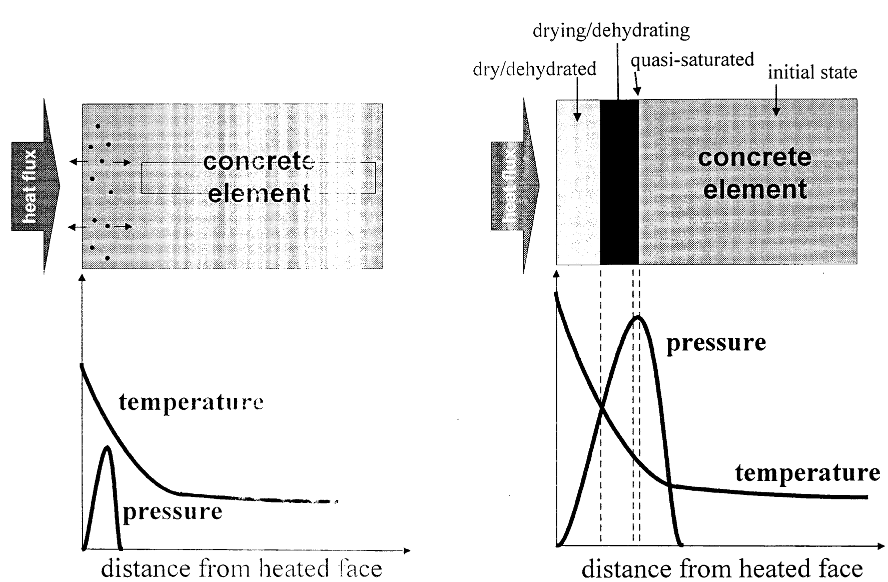


Fig. 1. The process for the build-up of pressure. Under the effect of pressure gradient, the water vaporized in the zone close to the heated face is transported (mainly by Darcy flow) not only towards the outside, but also the inside, of the concrete element at a lower temperature. It condenses again and a quasi-saturated layer is progressively formed, which impedes further mass transport in the inner direction.

the major driving force for mass transfer. Vapor and air are partially evacuated to the heated surface, but they also migrate to the center of the element, where vapor condenses again as soon as the thermodynamic conditions are satisfied. As a result a quasi-saturated layer is formed. After some time, the concrete element contains, from the heated surface, a dry and dehydrated zone, a drying and dehydrating zone and a quasi saturated layer that acts as an impermeable wall for gases. The remainder of the element is unchanged. The pressure peak is located at the saturated layer. The lower the permeability of the material, the sooner (and the closer to the heated surface) this moisture clog is generated and the higher the pressure and the pressure gradient.

This mechanism has never been quantified experimentally. This is the purpose of the experimental part of this paper.

### 2.2. Driving parameters in the spalling processes

The kinetics and the amplitude of the processes described above are controlled by the materials properties, as well as the characteristics of the structure element and those of the thermal and mechanical solicitations.

The material properties include heat and mass transfer properties (heat conductivity and heat capacity, permeabilities to vapor and liquid water) and mechanical properties (strengths, thermal creep, thermal dilation of the aggregates, etc.). These properties evolve significantly during the solicitation as a result of changes in the microstructure (porosity, pore size distribution, microcracking) [3,14,17–25]. The heat and mass transfer properties also depend strikingly on the moisture content of the material, especially in the initial state. The thermal dilation of the aggregates plays an important role in damage and varies significantly with its nature. For example, calcareous aggregates dilate less than siliceous ones.

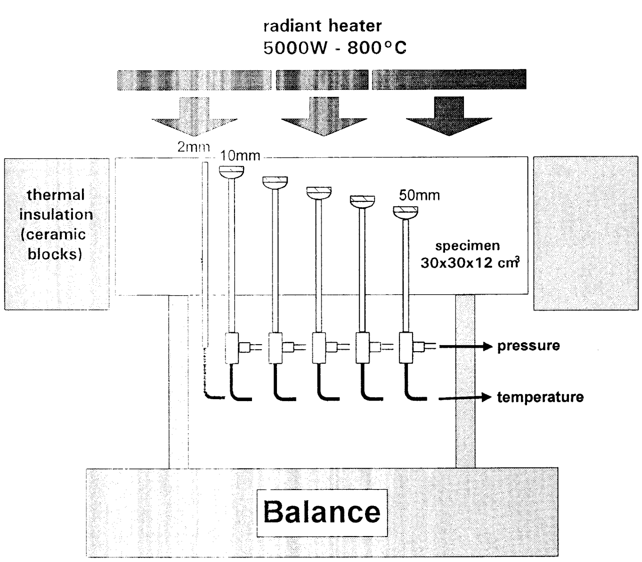


Fig. 2. The experimental set-up.

Table 1
Mixture proportions (kg/m$^3$) and compressive strength of concretes

| | M30 | M100-C |
|---|---|---|
| Water addition | 175 | 124 |
| High-range water reducing admixture (Résine GT, liquid) | – | 12.5 |
| Retarder (Chrytard, liquid) | – | 2.6 |
| Silica fume | – | 37.8 |
| Cement CPA — CEM I 52.5 | – | 377 |
| Cement CPJ — CEM II 32.5 | 350 | – |
| Silico-calcareous sand (Seine 0/4 mm) | 401 | 432 |
| Calcareous sand (Boulonnais 0/5 mm) | 401 | 439 |
| Calcareous aggregates (Boulonnais 5/12.5 mm) | 514 | 488 |
| Calcareous aggregates (Boulonnais 12.5/20 mm) | 514 | 561 |
| Water/cement or waterbinder | 0.50 | 0.34 |
| Nominal strength (MPa) | 34.9 ± 0.3 | 91.8 ± 0.8 |

At a larger scale, the size and the shape of the element also govern the temperature and moisture fields, therefore the whole thermo-hydro-mechanical history [2]. For example, the heat solicitation is much lower on a wall (1-D) than on a column (2-D). In addition, the vapor pressure may be much higher in a post. Moreover, the reinforcing bars may act as a thermal and mechanical discontinuity and cause premature spalling. On the other hand, as observed in the Channel tunnel, the reinforcement may hold back the concrete scales that act as a thermal shield and prevent further spalling.

Finally, the external solicitations have a critical effect on the spalling behavior of a concrete element. An external load or a pre-stress (especially with an eccentricity) enhances the risk of spalling. An external load may be generated during the fire as a result of the element dilation, constrained by the other elements of the structure. The thermal load is of course a determining factor; in most cases, the risk of spalling increases with the heating rate. However, there may be many exceptions to this. For example, a higher heating rate in a column may generate some macrocracks (thermo-mechanical damage), which would help to evacuate water from its core without reducing too much of its strength; at lower rates, the absence of macrocracks would make it impossible to evacuate water from the core and explosive spalling would occur. This type of spalling was observed in cylinders (Ø 16 cm) heated at only 1°C/min [2]. In addition, it is well known that most of the spalling activity lays between 250°C and 400°C, levels that are commonly reached in fire conditions.

This rapid overview brings to light that spalling is a complex phenomenon. Complexity stems from the coupling of the thermal, hydral, chemical and mechanical processes, rather than from the laws that govern these processes. It also shows that those processes are competing. For example, damage may help to increase permeability to evacuate water and reduce the pore pressure; but it also reduces concrete strength, thus increasing the spalling propensity. Although permeability is a key parameter, the effect of this parameter is correlated to the other ones, especially (but not only) initial water content. One should consider parameter correlations rather than parameters alone.

In other words, spalling is not a fully deterministic phenomenon. The risk of spalling is high in a range of configurations (mix, shape, loads, etc.) to be determined. The qualification of a given concrete element regarding fire behavior should be given in terms of both spalling probability and spalling type.

### 2.3. Methodology for the simulation of spalling

Let us remember that the main objectives of the studies on the behavior of HPC at high temperature are:

- To determine the thermo-mechanical constitutive laws of HPC structures in order to incorporate them in the calculation procedures of the codes (in particular the Eurocodes).
- To predict the risk of spalling of a structure and provide recommendations to prevent spalling.

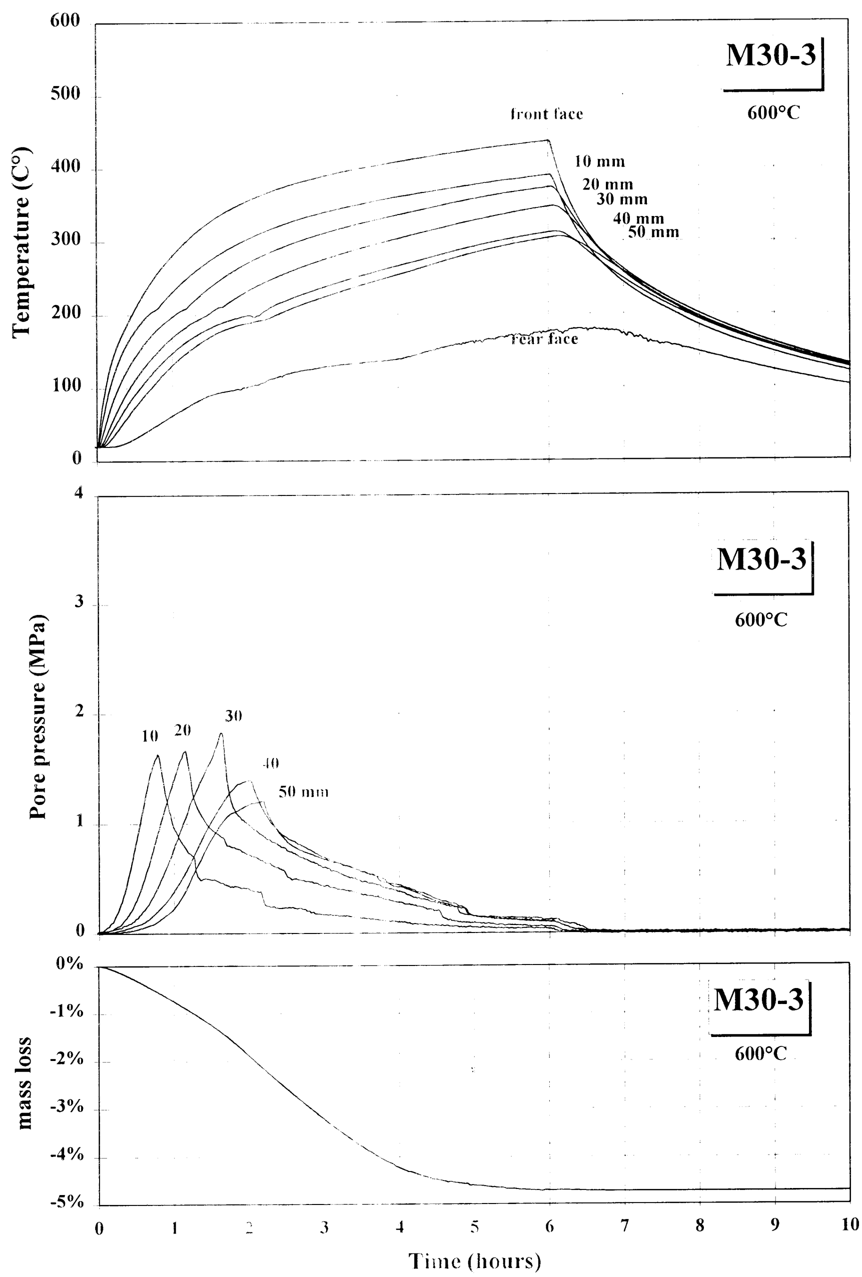


Fig. 3. M30, heated at 600°C. Mass loss and pressure and temperature fields vs. time.

From the engineer's point of view, these recommendations are in terms of concrete mix, nature and quantity of reinforcement and dimensions of the elements. The scientific methodology to provide these recommendations is in several steps.

The simulation of the thermo-hydro-mechanical process to spalling requires a numerical simulation. At the moment, no satisfying analytical approach could be developed. The numerical codes developed up to now [10,26–30] yield various fields: temperature, pore pressure and water content for the thermo-hydral part; if as HITECOSP code [26], the mechanical part is taken into consideration, damage, strain and stress fields are also predicted. This constitutes the first step. The experimental part of the present work provides numerical results to validate the thermo-hydral part of the codes.

In a second step, a spalling criterion was defined from those fields. This is the most difficult part; spalling is a local, stochastic and heterogeneous phenomenon, whereas all the fields mentioned above are a matter of continuum mechanics. Majorana et al. [26] propose a stress criterion. It has to be confirmed by experimental results, for example pressure measurements in elements that have spalled.

The last step for providing recommendations is to qualitatively and quantitatively determine the major parameters and parameter correlations regarding spalling. To the authors' knowledge, this parametric study remains to be done.

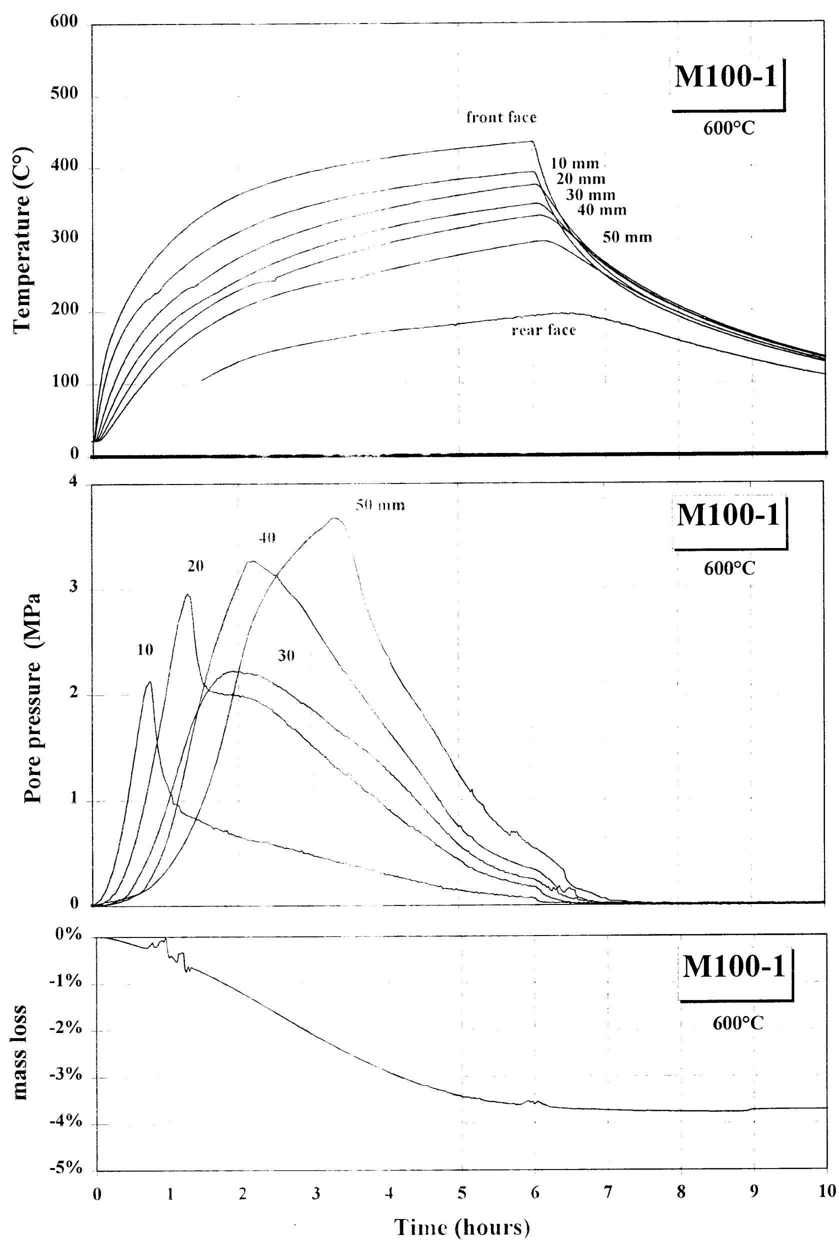


Fig. 4. M100, heated at 600°C. Mass loss and pressure and temperature fields vs. time.

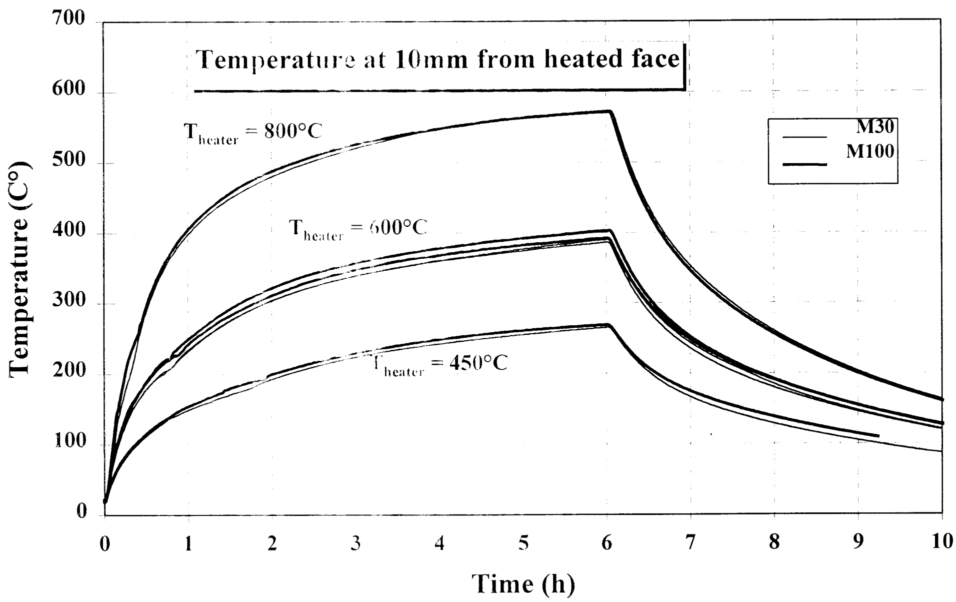


Fig. 5. Temperature at 10 mm from heated face vs. time, for all tests. M100 and M30 have a similar thermal behavior. This is also true at other depths.

### 2.4. Pore pressure measurements

Although pore pressure is a major field to understand the thermo-hydral process and validate the codes, very few experimental works were carried out. Pressure measurements were performed in sealed concrete at 171°C [31] and up to 600°C [32]. These works relate to the behavior of nuclear plant concrete vessels. The authors noted that pressure significantly exceeds the saturating vapor pressure. Kontani and Shah [32] showed the main role of the thermal dilation of liquid water on gas pressure. Consolazio et al. [27] measured pressures up to 31 bars in a mortar specimen heated on one face. This value was correlated to their model. On the contrary, Harada and Negishi [33] measured very low pressure values (2 bars) in a specimen heated to 900°C. This result is probably biased by the experimental procedure.

## 3. Experimental

The experimental work described in this paper aims at continuously measuring temperature and pores pressure fields, as well as mass loss, in a prismatic specimen subjected to a quasi-unidirectional thermal load. The results contribute to understanding the thermo-hydral processes that take place at high temperatures.

### 3.1. The set-up

The thermal load is applied on one face of a prismatic concrete specimen ($30 \times 30 \times 12$ cm$^3$), whereas the lateral faces of the specimen are heat-insulated with porous ceramic blocks. Heating is provided by means of a radiant heater (up to 5 kW and 800°C) that covers the surface of the specimen, placed 3 cm above it (Fig. 2).

The specimen is placed on a balance in order to monitor its mass during heating. A retention tray is placed between the specimen and the balance for retaining water that may come out from the rear face of the specimen.

The specimens were instrumented with six gauges placed at casting, for simultaneous pressure and temperature measurements. These gauges are made of a sintered

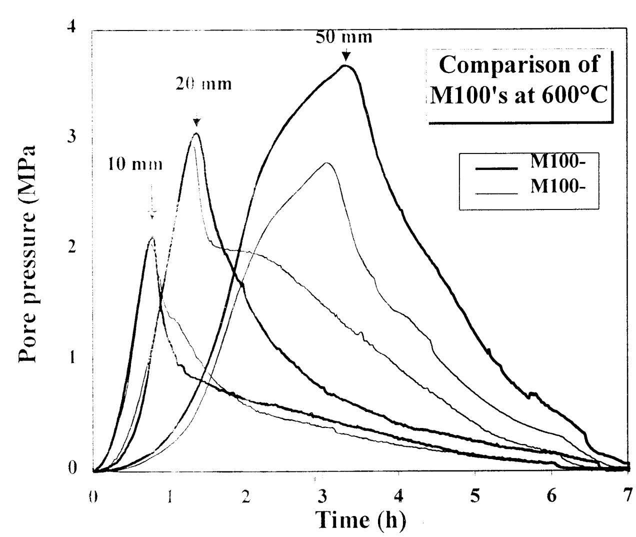


Fig. 6. Pressure vs. time for M100s at 600°C. The tests present a fairly good repeatability, considering the processes involved for the build-up of pressure. The low peak of M100-3 at 50 mm may be due to a leak observed on the 40-mm gauge.

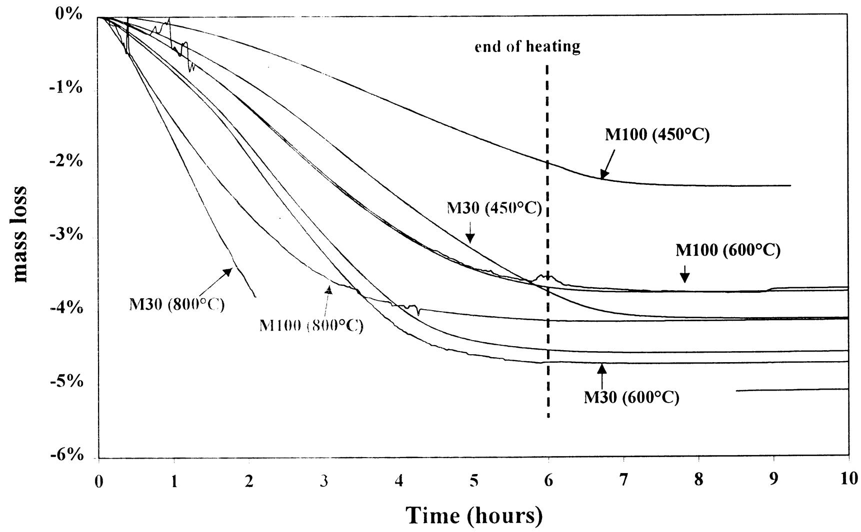


Fig. 7. Mass loss vs. time for all tests. As expected, the rate and amplitude of mass loss are larger for M30 and increase with the temperature of solicitation.

metal round plate (Ø 12 × 1 mm) crimped in a metal cup. The latter is brazed to a thin metal tube (inner diameter 1.6 mm), which comes out of the rear face of the specimen. At the time of testing, a tight connector is placed at the free end of the tube. It firstly connects the gauge to a piezoelectric pressure transducer through a flexible tube filled with silicone oil. Secondly, a thermocouple (Ø 1.5 mm) is inserted in the tube through the connector down to the metal plate. The free volume of the gauge is around 250 $mm^3$. This alters slightly the measured pressure values. However, as we shall see in the following, water is transferred in the specimen during heating and saturates this volume with liquid water. Therefore, pressure is slightly underestimated and measured with some time lag. This may cause problems at very high heating rates, which is not the case in our experiments.

Five gauges were placed in the central square zone of $10 \times 10$ $cm^2$, at 10, 20, 30, 40 and 50 mm from the heated surface, respectively (Fig. 2). The sixth gauge is made of a plain tube, the end of which is located at 2 mm from the heated surface for measuring its temperature. Both thermocouples and pressure tubes are very loose so that they do not disturb mass measurements.

### 3.2. Mixes and experimental conditions

The tests were carried out on two mixes: an ordinary concrete (OC; M30, w/c = 0.5) and a HPC (M100, w/c = 0.32), both made with calcareous aggregates. Their composition and characteristics are given in Table 1. A comprehensive analysis of the thermal and hydral properties of those concretes at high temperature was performed earlier and is reported in [34]. The specimens were kept in a sealed bag for about 6 months. Their moisture state was therefore homogeneous. The latter was measured on small specimens fabricated at the same time and stored in the same conditions. They were dried at 105°C until achieving steady mass.

The tests were performed in a temperature range where spalling may occur: the temperature of the radiant heater was 450°C, 600°C and 800°C, respectively. In each case, a step signal was applied. At 800°C, the specimens exhibited very large cracks on their sides (perpendicular to them and to the heated surface), through which a large amount of vapor escaped. The 1-D condition was no longer satisfied and except at 10 mm, the pressure measurements are not valid. M100 at 800°C is the only specimen that exhibited some spalling: scales 1–2 cm wide and up to 5 mm thick. The tests were duplicated at 600°C, and one test was performed at 450°C. This provides two different conditions for validating the numerical codes.

## 4. Results and analysis

### 4.1. Overview of the results

Figs. 3 and 4 give an overview of the results as they come out of the computer at the end of the test. The temperature, pressure and mass loss vs. time curves refer to a 600°C test, however, they are representative of the 450°C.

Table 2
Mixes and main characteristics of concretes

| | M30 | M100 |
|---|---|---|
| Initial water content (% mass) | 3.9 | 2.95 |
| Initial degree of saturation of the pores $u_{liq}(293)$ (vol.%) | 63 | 77 |
| Initial porosity (%) | 14.3 | 9.4 |
| Porosity at 200°C(%) | 15.8 | 9.4 |
| Degree of saturation at 220°C $u_{liq}(493)$ (%), taking into account liquid water dilation | 69 | 91 |

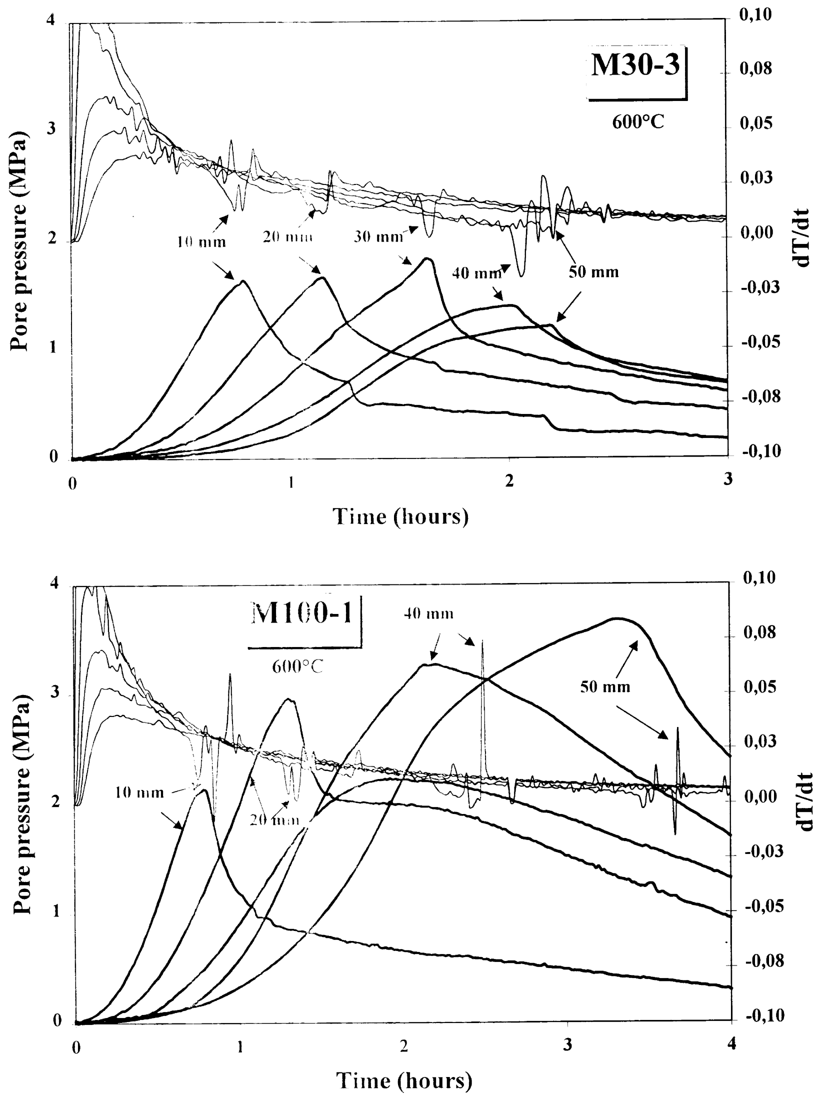


Fig. 8. M30 and M100 at 600°C. Pressure and temperature derivative vs. time. The peaks on the d*T*/d*t* curves (corresponding to the plateau on the temperature curves) are located at the pressure peak (M30) or close after it (M100). This phenomenon confirms that a quasi-saturated layer precedes the drying front.

At each depth, the temperature increases smoothly with time. However, the curves exhibit a small plateau around 200°C for M30 and 230°C for M100. Moreover, the thermocouple placed in contact with the rear (unheated) face of the M30 specimens brought to light the occurrence of two plateaus, at 100°C and 130°C. These plateaus yield worthwhile information of the hydral behavior of the specimens, as we shall see in the following.

Both concretes have a similar thermal behavior, as observed in Fig. 5 where the 10-mm curves of all tested specimens where plotted. This is not surprising since they have similar thermal properties [34].

Whereas temperature increases smoothly, the pore pressure curves exhibit a very well marked peak. Pressure reaches up to 37 bars in M100 (at 50 mm), whereas it does not exceed 18 bars in M30. This marked difference

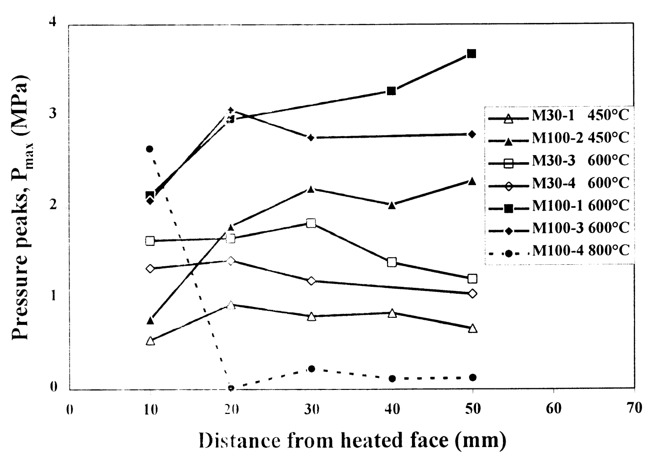


Fig. 9. Pressure peaks ($P_{max}$) vs. distance to the heated face. For M100 (800°C), only the 10-mm point is valid because this specimen underwent macrocracks through which vapor could escape.

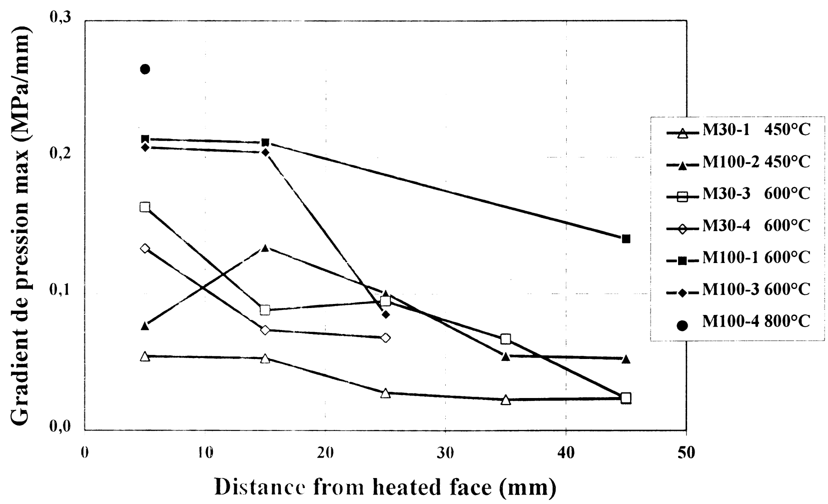


Fig. 10. Maximum pressure gradient (absolute value) at each depth for all tests. The larger gradients are located within 20 mm from the heated face. They are larger for M100 and at higher temperatures.

between ordinary and HP concrete will be analyzed in the following. Some anomalies were observed in the pressure curves, e.g. the 30-mm curve in Fig. 4 is not consistent with the 20- and 40-mm curves. In most cases, it was identified that an o-ring in the connector had been damaged, which resulted in a leak. In the other cases, the anomaly may result from a crack formed at the interface between the pressure gauge and the concrete. Vapor could escape through this crack. Despite this, the tests that were duplicated showed a fairly good repeatability, as observed in Fig. 6.

At last, the heating process resulted in a mass loss (mainly water), as shown in the bottom curves of Figs. 3 and 4. All mass loss curves are gathered in Fig. 7. Some curves exhibit a disturbance, due to the friction between the insulating blocks and the specimen. This was fixed during the test; therefore, the rest of the curve is valid. For each heating condition, the total mass loss is higher in M30 than in M100, due to the larger initial water content of M30 (Table 2). Moreover, the rate of mass loss is always higher in M30, as a result of its higher permeability [34].

### 4.2. Pressure fields

An interesting feature of the tests appears when correlating the time derivative of the temperature with pressure (Fig. 8). The Dirac-like peaks in the d$T$/d$t$ curves indicate the small plateaus observed in Figs. 3 and 4. In M30, they occur exactly at the same time as the peaks on the pressure curve. In M100, the Diracs appear either at the same time or shortly after the pressure peak. This plateau on the tem-

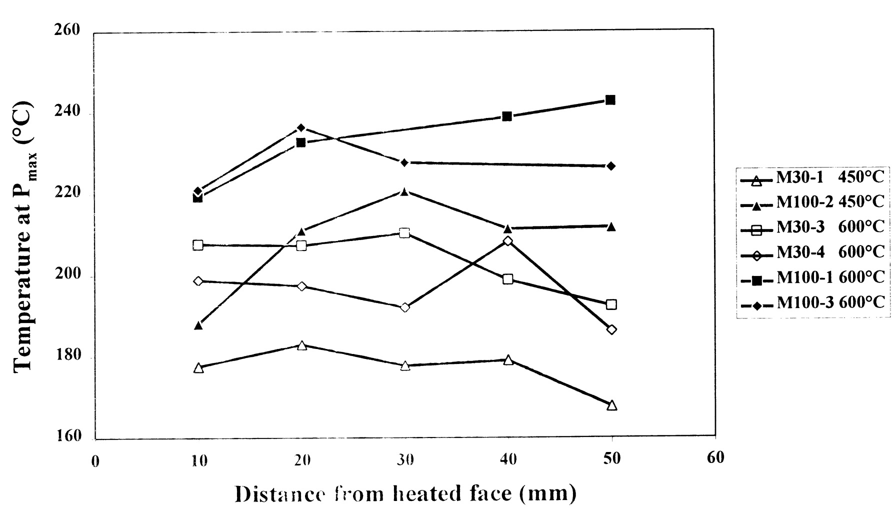


Fig. 11. Temperature at $P_{max}$ vs. distance to heated face. $T_{P_{max}}$ evolves similarly to $P_{max}$, but in a narrow range.

perature curve corresponds to an important energy consumption, the origin of which is water vaporization. Then, this phenomenon brings to light that the pressure peak is associated with the vaporization and the transport of an important amount of water. This is made possible because the permeability of the concrete slice located between the pressure peak and the heated surface is high enough. It increased because concrete was damaged by drying and dehydration. These experimental observations confirm the hypothesis that the drying/dehydration front is preceded by a quasi-saturated zone, formed by migration of vapor, which condenses when thermodynamic conditions are satisfied. However, it is possible that this phenomenon was enhanced by the presence of free volume in the gauge, which may act as a water reservoir. Future tests will address this matter.

On the curve related to the rear face of M30 specimens, two plateaus are visible (Fig. 3): the first one around 100°C corresponds to the vaporization of water initially present at that location; the second one around 120°C appears when the drying front reaches the rear face of the specimen. None of these plateaus is visible in M100 due to slower drying rates.

The most striking difference between M30 and M100 lays in the height of the pressure peaks, as observed in Fig. 9. For example, at 600°C, $P_{max}$ reaches 37 bars at 50 mm in M100 (at 50 mm), whereas it never exceeds 18 bars in M30 (at 30 mm). Moreover, the pressure gradients are higher in M100 than in M30 (Fig. 10). This explains for a major part why HPC is more subject to spalling at high temperature.

In M100, $P_{max}$ increases with depth. This increase is bigger up to 20 mm. On the other hand, in M30, $P_{max}$ is almost stable up to 30 mm, then decreases. This behavior of M30 is due to its high permeability: both the rear face and the front face of the specimen influence moisture transport. The temperature at $P_{max}$, noted $T_{p_{max}}$ follows the same trend, however, in a narrow temperature range (Fig. 11). For example, at 600°C, the pressure peaks occur between 220°C and 240°C in M100, and between 190°C and 210°C in M30. $T_{p_{max}}$ is always lower by 20–40°C in M30 than in M100. However, the saturating vapor pressure varies strikingly with temperature in this range, as we shall see in the following. The 10-mm point for M100 at 800°C appears in Figs. 9 and 10. The high values of pressure and pressure gradient lead us to suspect that very high pressures would have been reached at larger depths and/or more spalling would have occurred, if the side effect (macrocracks) had not been dominant.

## 5. Discussion: pressure–temperature diagrams

The analysis of the thermodynamic diagrams (pressure vs. temperature) enlightens the difference between M30 and M100 regarding pressure peaks. Fig. 12 shows those diagrams for M30 and M100 at 600°C, together with the saturating vapor pressure $P_{vs}(T)$. Furthermore, the ($P_{max}$, $T_{p_{max}}$) couples for every test were gathered in Fig. 13.

As observed in the previous paragraph, the temperature at pressure peaks is only 20–40°C lower in M30 than in M100. However, $P_{vs}(T)$ increases strikingly with temperature in this range. This partly explains why pressure peaks are much higher in M100 than in M30.

The differences between the experimental pressure curves and the saturating vapor pressure express the other phenomenon observed in Fig. 12. In M30, the experimental curves are very close to $P_{vs}(T)$, whereas they are far above it in M100. The largest difference does not exceed 2 bars in M30, whereas it rises up to 8 bars in M100 (at 50 mm). The contribution of vapor to the total pore pressure $P_{tot}(T)$ is $P_{vs}(T)$. The overpressure is attributed to the

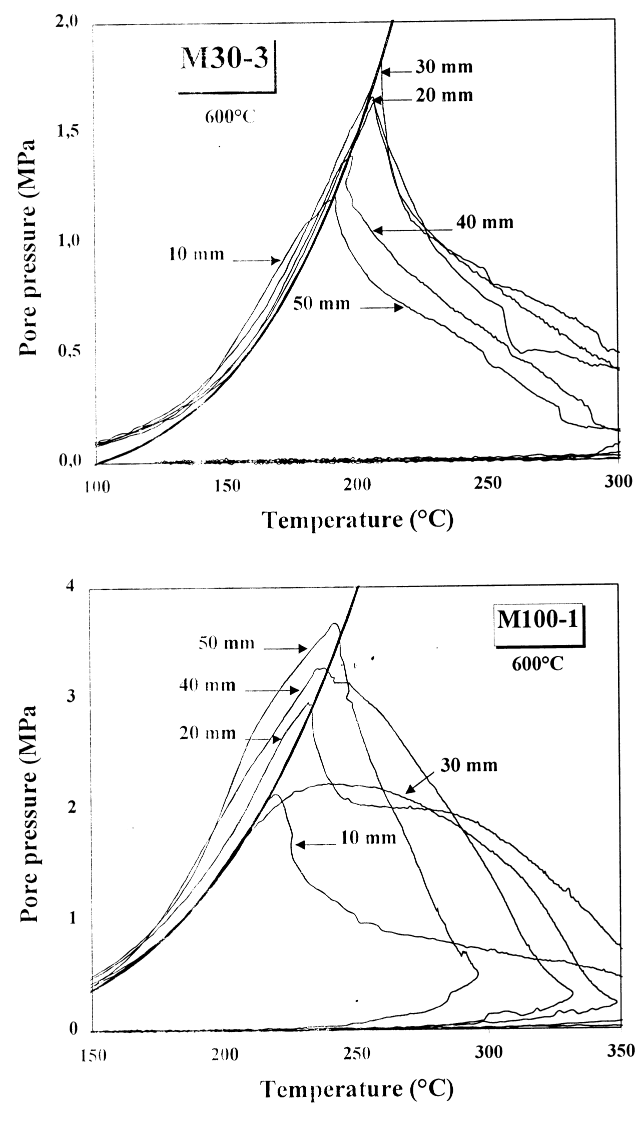


Fig. 12. Pressure vs. temperature diagrams for M30 and M100, plotted together with the saturating vapor pressure $P_{vs}(T)$. In M30, the pressure is very close to $P_{vs}(T)$. This is not the case in M100.

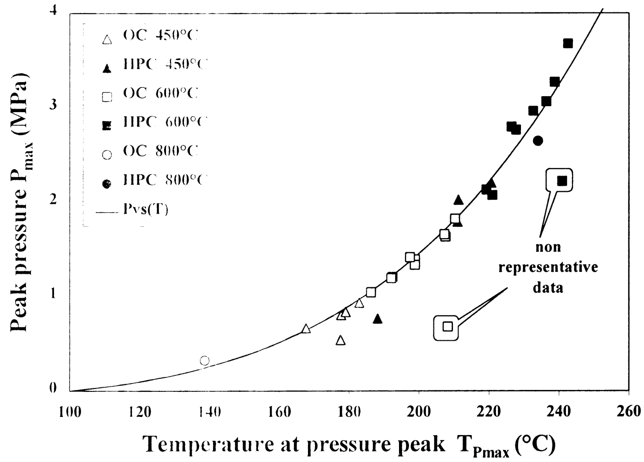


Fig. 13. $P_{max}$ vs. temperature at $P_{max}$ for all tests. The data points are very close to $P_{vs}(T)$. M30 and M100 constitute two different classes.

partial pressure of the air enclosed in the porous network [see Eq. (1)]:

$$P_{air}(T) = P_{tot}(T) - P_{vs}(T) \quad (1)$$

When the pressure approaches the peak value, the pressure curve meets $P_{vs}(T)$. This means that all the enclosed air was evacuated and that vapor is the only remaining gas. The overpressure increases with the distance from the free surface because the mass transfer is more difficult. The simple calculation hereafter shows that $P_{air}(T)$ does not follow the perfect gas law. The porous network is made of three phases: liquid water, vapor and air. The perfect gas law yields Eq. (2)

$$P_{air}(T) = \frac{nRT}{V_{air}(T)} = \frac{nRT}{V_{pore}(T) - V_w(T)} \quad (2)$$

where $n$ is the number of moles of air, $R$ the perfect gas constant and $V_{pores}$, $V_{air}$ and $V_w$ the volume of the pore, of air and liquid water, respectively. Referring to the initial conditions, $P_{air}(T)$ is expressed as [Eq. (3)]

$$P_{air}(T) = P_{air}(293)\frac{T}{293}\left(\frac{1 - u_{liq}(293)}{1 - u_{liq}(T)}\right) \quad (3)$$

where $T$ is expressed in degrees Kelvin and $u_w = ((V_w)/(V_{pore}))$ is the degree of saturation of the pore. Additionally,

$$u_w(T) = \frac{d_c(T)}{d_w(T)}\frac{\theta_{ini}}{\varepsilon(T)} \quad (4)$$

where $d_c$ and $d_w$ are the density of concrete and water, $\varepsilon$ is the porosity and $\theta_{ini}$ is the initial mass water content. These values are given in Table 2. Eq. (4) assumes that the pore water content at $T$ is equal to the initial value.

Table 3
Parameters necessary for the calculation of $P_{air}$(220°C)

| | |
|---|---|
| Total pressure ($P_{tot}$) at 20°C (bars) | 1.013 |
| Saturating vapor pressure ($P_{tot}$) at 20°C (bars) | 0.023 |
| $P_{air}$ at 20°C (bars) | 0.99 |
| Density of water at 220°C [15] | 0.83 |

Table 4
Comparison between calculated and experimental values of $P_{air}$ at 220°C

| | M30 | M100 |
|---|---|---|
| $P_{air}$ at 220°C without taking into account water dilation (bars) | 1.7 | 1.7 |
| $P_{air}$ at 220°C taking into account water dilation (bars) | 2 | 4.5 |
| Experimental value of $P_{air}$ at 220°C (bars) | 1.9 | 8.1 |

Despite the higher initial water content in M30, the initial degree of saturation of M100 (77%) is higher than that of M30 (62%). As a consequence, the effect of water dilation [35] is bigger in M100 than in M30: At 220°C, the degree of saturation reaches 91% in M100 vs. 69% in M30. The volume available for air and vapor was therefore divided by 2.6 in M100, whereas it barely changed in M30. This results in a strong influence on the calculated air pressure in M100 ($P_{air}(220) = 4.5$ bars) and a weak one in M30 ($P_{air}(220) = 2$ bars).

The calculated and measured values are very close for M30 (Table 3). On the other hand, for M100, the measured value is two times greater than the calculated one. This shows that the hypothesis made in Eq. (4) is not valid: Water was transferred towards the inside of the specimen under the effect of the pressure gradients and provided a higher degree of saturation. This confirms that a quasi-saturated layer is formed during the drying process and acts as a barrier to vapor. Spalling was also observed at lower initial water content. The amount of water available in concrete (especially chemically bound water) is very high compared to that necessary to form the layer (Table 4).

## 6. Conclusions

An original experimental set-up was used to perform pore pressure measurements in HPC and OC specimens subjected to high temperatures, in conjunction with temperature and mass loss. The results yielded important information on the thermo-hydral processes that lead to spalling and will be very useful to validate the numerical codes, although the thermal conditions were much less severe than that of the standard solicitation. The main trends observed are the following.

- M30 and M100 have globally a similar thermal behavior, consistent with their similar thermal properties (thermal conductivity and specific heat).
- For both concretes, pore pressure curves exhibited a well-marked peak. The level of this peak was much higher in M100 than in M30: up to 38 bars was measured in M100 vs. 18 bars in M30. These values are slightly underestimated, considering the way they were measured.
- As well, M100 underwent higher pressure gradients than M30. The latter increased with the temperature of

solicitation and were higher within 20 mm from the heated face. This is consistent with the thickness of the scales observed in progressive spalling.

- A small plateau was observed on the temperature vs. time curves in the neighborhood of 200°C. It was demonstrated that this occurs at the same time as the pressure peak in M30 and slightly after in M100. This plateau expresses that a large amount of water was vaporized. The thermodynamic conditions for this vaporization were met, thanks to the degradation of the material, allowing mass transfer.
- The pressure vs. temperature curves also yielded important information: In M30, they stayed very close to the saturating vapor pressure, whereas in M100, pressure reached values much higher than $P_{vs}(T)$. This overpressure is attributed to the partial pressure of the air enclosed in the pores. It increased under the direct effect of temperature (perfect gas law), but it was demonstrated that the main effect was the decrease in the volume available for gases in the pores due to both the dilation of liquid water and the amount of water that was brought in from the drying zone.
- The temperature at the pressure peak was very close to $P_{vs}(T)$. It was only 20–40°C higher in M100 than in M30 (it laid around 180°C to 240°C), but in this temperature range, $P_{vs}(T)$ varies strikingly with temperature. As a consequence, M100 underwent much higher pore pressures than M30.

Globally, this analysis shows that the pressure release after the peak corresponds to the drying-dehydration front passing through, and lets one suppose that this front is preceded by a quasi-saturated layer that acts as a moisture clog. This layer is generated by vapor transferred from the drying zone to the inside of the specimen under the influence of pore pressure gradients. The thermal dilation of liquid water is also significantly involved is this process. The difference between M30 and M100 is made clear: As a consequence of lower permeabilities (to vapor and liquid water), there is a large difference in the thermodynamic conditions reached in the porous network, which results in much higher pore pressures.

## Acknowledgment

This work was supported by the French National Project BHP 2000.

## References

[1] K. Hertz, Heat-induced explosion of dense concretes, Technical University of Denmark, Institute of Building Design Report No. 166, 1984.

[2] A. Noumowe, P. Clastres, G. Debicki, M. Bolvin, Effect of high temperature on high performance concrete (70–600°C) — strength and porosity, in: V.M. Malhotra (Ed.), Third CANMET/ACI International Conference on Durability of concrete, Nice (France) (1994) 157–172.

[3] U. Diederichs, U.-M. Jumppannen, V. Penttala, Behaviour of high strength concrete at high temperatures, Espoo 1989, Helsinki University of Technology, Department of Structural Engineering, Report 92, 1992, pp. 15–26.

[4] D.E. Allen, T.T. Lie, Fire resistance of reinforced concrete columns and walls, in: NRCC (Ed.), Proceedings of Canadian Structural Concrete Conference, Ottawa (Canada) June, 1977, pp. 17–33.

[5] L.A. Ashton, S.C.C. Bate, The fire-resistance of prestressed concrete beams (Paper No. 6444), in: T. TelFord (Ed.), Proc Inst Civ Eng, Vol. 17, (London) 1960, pp. 15–38.

[6] J.-J. Jensen, E.A. Hansen, U. Danielsen, S. Seglem, Offshore concrete structures exposed to hydrocarbon fire. in: University of Edinbourg (Ed.), The First International Conference on Concrete for Hazard Protection, Edinbourg (Germany), 1987, pp. 147–159.

[7] G. Sanjayan, L.J. Stocks, Spalling of high strength silica fume concrete in fire, ACI Mater J 90 (2) (1993) 170–173.

[8] I.W.J. Copier, The spalling of normalweight lightweight concrete on exposure to fire, Heron 24 (2) (1979) 3–92.

[9] R. Breitenbücker, High strength concrete C 105 with increased fire resistance due to polypropylene fibres, in: F. de Larrard, R. Lacroix (Eds.), 4th International Symposium on Utilization of High-Strength/High-Performance Concrete, Paris (France) 1996, pp. 571–577.

[10] F.J. Ulm, O. Coussy, Z.P. Bazant, The "Chunnel" fire: I. Chemoplastic softenning in rapidly heated concrete, J Eng Mech 125 (3) (1999) 272–282 (March).

[11] Z.P. Bazant, M.F. Kaplan, Concrete at high temperatures, Material Properties and Mathematical Models, Longman, Burnt Mill, England, 1996.

[12] Z. Sawicz, Z. Owsiak, Effect of temperatures on the hydrated cement pastes, in: University of Brno (Ed.), Proceedings of the 5th Symposium on Science and Research in Silicate Chemistry, Brno (Czechoslovakia), 1981, pp. 56–67.

[13] F.M. Lea, The Chemistry of Cement and Concrete, in: E. Arnold (Ed.), London 1970, pp. 196–201.

[14] M. Tsimbrovska, P. Kalifa, D. Quenard, J.F. Daïan, High performance concrete at elevated temperature: Permeability and microstructure, in: M. Livolant (Ed.), Transactions of the 14th International Conference on Structural Mechanics in Reactor Technology, Vol. 5, Lyon (France), (1997) pp. 475–482.

[15] T.Z. Harmathy, Effect of moisture on the fire endurance of building element, National Research Council, Research paper No. 270 of the Division of Building Research, Ottawa, Canada, 1965.

[16] Y. Anderberg, Spalling phenomena of HPC and OC, in: L.T. Phan, N.J. Carino, D. Duthiuh, E. Garboczi (Eds.), Proceedings of the International Workshop on Fire Performance of High-Strength Concrete, NIST, Gaithersburg (USA), 1997, pp. 69–73.

[17] K. Hertz, Heat-induced explosion of dense concretes, Technical University of Denmark, Institute of Building Design, Report No. 166, 1984.

[18] P. Kalifa, M. Tsimbrovska, V. Baroghel-Bouny, High performance concrete at elevated temperatures — an extensive experimental investigation on thermal, hygral and microstructure properties, in: P.C. Aïtcin, Y. Delagrave (Eds.), Proceedings of the International Symposium on High-Performance and Reactive Powder Concretes, Sherbrooke (Canada), 1998, pp. 259–279.

[19] R. Felicetti, P.G. Gambarova, Effects of high temperature on the residual compressive strength of high-strength siliceous concretes, ACI Mater J 95 (4) (1998) 395–406.

[20] R. Felicetti, P.G. Gambarova, Residual capacity of HSC thermally damaged deep beams, J Struct Eng 319 (1999) 319–327.

[21] C. Castillo, A.J. Durrani, Effect of transient high temperature on high-strength concrete, ACI Mater J 87 (1) (1990) 47–53 (Jan.–Feb.).

[22] A.N. Noumowe, P. Clastres, G. Debicki, J.L. Costaz, High performance concrete for severe thermal conditions, in: K. Sakia, N. Banthia, O.E. Gjørs (Eds.), Proceedings of the International Conference on Concrete Under Severe Conditions, CONSEC'95, Vol. 2, Sapporo (Japan), 1995, pp. 1129–1140.

[23] V.M. Malhotra, V.S. Ramachandran, R. Feldman, P.C. Aïtcin, Condensed Silica Fume in Concrete, CRC Press, Boca Raton, Florida, 1987, p. 167.

[24] G.A. Khoury, B.N. Grainger, G.P.E. Sullivan, Transient thermal strain of concrete: Literature review, conditions within specimen and behavior of individual constituents, Mag Concr Res 37 (132) (1985) 131.

[25] G.A. Khoury, Compressive strength of concrete at high temperature: A reassessment, Mag Concr Res 44 (161) (1992) 291.

[26] C. Majorana, V. Salomoni, B. Schrefler, Hygrothermal and mechanical model of concrete at high temperature, Mater Struct 31 (210) (1998) 378.

[27] G.R. Conzolazio, M.C. McVay, J.W. Rish III, Measurement and prediction of pore pressures in saturated cement mortar subjected to radiant heating, ACI Mater J 95 (5) 1998.

[28] G.N. Ahmed, P.J. Hurst, An analytical approach for investigating the causes of spalling of high-strength concrete at elevated temperatures, in: L.T. Phan, N.J. Carino, D. Duthiuh, E. Garboczi (Eds.), Proceedings of the International Workshop on Fire Performance of High-Strength Concrete, NIST, Gaithersburg (USA), February, 1997, pp. 95–113.

[29] Z.P. Bazant, W. Thonguthai, Pore pressure and drying of concrete at high temperature, Proc ASCE J Eng Mech Div 104 (1978) 1058–1080.

[30] Z.P. Bazant, W. Thonguthai, Pore pressure in heated concrete walls: Theoretical prediction, Mag Concr Res 31 (107) (1977) 67–76.

[31] G.L. England, R.J. Greathead, S.A. Khan, Influence of high temperature on water content, permeability and pore pressures in concrete, in: H. Shibata (Eds.), SMIRT 11 Transactions Vol. H, Tokyo (Japan), August 1991.

[32] O. Kontani, S.P. Shah, Pore pressure in sealed concrete at sustained high temperatures, in: Proceedings of the International Conference On Concrete Under Severe conditions, CONSEC'95, Sapporo (Japan) Vol. 2, (1995) 1151–1162.

[33] K. Harada, K. Negishi, Spalling of cement mortar during fire, in: K. Watanabe (Ed.), Proceedings of the Workshop on Modelling of Deterioration in Composite Building Components due to Heat and Mass Transfer, Tsukuba, Japan, 1998, pp. 171–182.

[34] P. Kalifa, M. Tsimbrovska, V. Baroghel-Bouny, High performance concrete at elevated temperatures — an extensive experimental investigation on thermal, hygral and microstructure properties, in: P.C. Aïtcin, Y. Delagrave (Eds.), Proceedings of the International Symposium on High-Performance and Reactive Powder Concretes, Sherbrooke (Canada), 1998, pp. 127–143.

[35] D.J. Furbish, Fluid Physics in Geology. An Introduction to Fluid Motion on Earth Surface and Within Its Crust, Oxford Univ. Press, Oxford (UK) 1997.